Research Article

Study of Isotherm and Kinetics for Remediation of Congo Red Using Nanocomposite Bead

Pankaj Sarkar, Swagatam Sarkar, Dhiman Santra, Shanku Denrah, Mitali Sarkar[*]

Department of Chemistry, University of Kalyani, Kalyani 741 235, India
Email: msarkar@klyuniv.ac.in

Abstract: Cellulose-based nanocomposite (FeCNB) has been synthesized via sol-gel conversion for adsorptive remediation of Congo red, a carcinogenic and mutagenic azo dye, from water. The bead was characterized by Fourier transform-infrared (FT-IR), scanning electron microscopy (SEM), field emission scanning electron microscopy (FESEM), energy dispersive X-ray analysis (EDAX) and transmission electron microscopy (TEM). The effect of adsorbent dose, pH, contact time, shaking speed, initial dye concentration and temperature was carried out in a batch adsorption study. The maximum removal of Congo red was found at pH 6.0, corresponding to the adsorbent dose of 1.0 gdm^{-3} and 90 min of contact time. The experimental data were analyzed using different isotherm and kinetic models. The data was fitted best to Langmuir isotherm model and pseudo-second-order kinetic model. The maximum adsorption capacity evaluated from Langmuir isotherm is 3.52 mgg^{-1} at 303 K. Thermodynamic study was carried out to evaluate the changes in Gibbs free energy (ΔG^0), enthalpy (ΔH^0) and entropy (ΔS^0) of the dye-adsorbent interaction. The negative ΔG^0 values at all temperatures suggested the spontaneous nature; the positive ΔH^0 value indicated the endothermic nature and the positive ΔS^0 indicated the increased randomness of the adsorption process. Desorption study found 0.1 (M) NaOH as the most suitable eluting agent for dye-loaded adsorbent. The adsorbent can be used up to five successive cycles of adsorption-desorption.

Keywords: Congo red, FeCNB, adsorpticve remediation, batch adsorption, desorption

1. Introduction

Dyes are the chemical substances that impart colour to textiles, leather, paper, or any other materials and this colouring is not generally altered by washing or when exposed to sunlight, heat, or any other factors.[1] Until the 1850s, dyes were originally derived from natural sources such as plants, trees, fungi, vegetables, insects, etc. Moreover, barks, leaves, or roots of selected trees or plants were widely used as a source of natural dyes.[1] A great problem for older fabric dyes was their poor colour fastness. These dyes are washed out easily from fabric.[1] So, the development of proper mordant was a great challenge to researchers. After the discovery of mauve, the first synthetic dye, researchers have paid more attention to synthesize more and more synthetic dyes due to their use in industries. A large amount of unfix dyes are released to environment causing a serious environmental pollution. Increased concentration of dyes in water bodies highly affects the aquatic ecosystem. About 7.0×10^5 tonnes of synthetic dyes are produced globally of which 60% dyes

are azo dyes.[2,3] Azo dyes and their degradation products are found to be highly toxic and poor biodegradability.[4]

Congo red is an organic synthetic azo dye. It was the first synthetic dye that did not require any mordant to stain textile fibres.[5] It was formerly used to dye cotton for imparting bright red colour, but nowadays, it has been suppressed by some synthetic dyes, more resistant to washing and sunlight. Congo red is extensively used in textile, rubber, plastic, textile, and paper industries.[6] The use of this dye has been banned in certain countries due to its carcinogenic nature. However, this dye is still used in histology to stain tissues of microscopic systems for demonstrating the presence of amyloidosis. It is an irritant to human's skin, eyes, and aquatic biota and can induce somnolence and respiratory problems.[7] The carcinogenic and mutagenic effect of Congo red has also been reported by researchers. The dye was also found to be toxic for several aquatic biota such as microalgae, cladocerans, and zebrafish.[8] The general information viz: IUPAC name, type of dye, molecular formula, molecular weight, physical appearance and structure of CR are represented in Table 1.

Table 1. General information of Congo red (CR)

IUPAC name	Disodium 4-amino-3-[4-[4-(1-amino-4-sulfonato-naphthalen-2-yl) diazinylphenyl]phenyl] diazenyl-naphthalene-1-sulfonate
Type	Azo dye
Molecular formula	$C_{32}H_{22}N_6Na_2O_6S_2$
Molecular weight	696.665 gmol^{-1}
Physical appearance	Brownish red powder
Chemical structure	
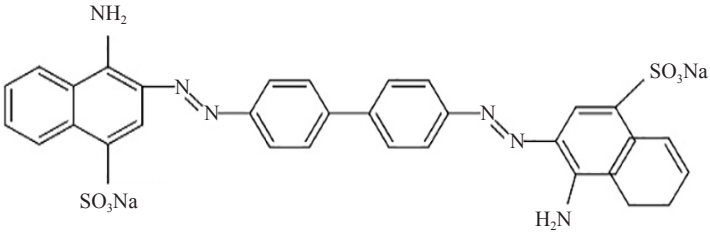
Several removal techniques such as Fenton oxidation[9,10], ozonation[11,12], membrane separation[13], coagulation-flocculation[14], adsorption[15-17] etc., have been employed for the decontamination of Congo red from aqueous solution. Fenton process is quick and time saving with high efficiency towards water soluble and insoluble contaminants. This process requires careful monitoring and may produce large amount of hazardous sludge. Ozonation is another popular time saving and effective technique which does not produce sludge. However, it requires expensive equipment, careful monitoring, and high voltage for continuous ozonation to the sample solution. Membrane filtration can effectively remove the dye from the sample solution, but it is a time-consuming process with limited flow rate.

Adsorption is comparatively simple, cost effective and feasible technique. The development of adsorbents from natural and biomaterials can make the process further cost-effective. A large number of synthetic dyes including Congo red can be treated/removed from water and wastewater using the adsorption technique.[15-17]

The choice of adsorbent has great importance in the removal of Congo red by adsorption technique. Low-cost biological materials have been extensively used for decontamination of Congo red. Cellulose is one of the most important biomaterials chosen as starting material because of its easy availability compared to other biomaterials. Nano-materials provide more surface area compared to the corresponding microscopic state and thereby capable of more adsorbate molecules in its surface.

In the present study, attention has been paid to synthesize a nanobiocomposite from cellulose as it is an environmentally safe natural product. It is the most abundant natural polysaccharide, is plenty available in nature. In order to increase the efficiency of the adsorbent, cellulose powder was first converted to nano cellulose bead by

xanthation followed by sol-gel conversion. Cellulose nanocomposite bead (CNB) was finally modified with Fe(III) solution to produce the desired adsorbent FeCNB, expecting to have higher removal efficiency for CR.

2. Materials and methods

2.1 *Reagents and materials*

Analytical grade solvents and chemicals were used in this study. Cellulose powder and Congo red (CR) were purchased from Loba Chemie, India and Merck, India respectively. A 250 mgdm^{-3} stock solution of Congo red was prepared using deionized water. Fe(III) nitrate (Merck, India) solution was used to convert cellulose nanocomposite bead (CNB) to Fe(III) loaded cellulose nanocomposite bead (FeCNB).

2.2 *Synthesis of the adsorbent*

The synthesis of Fe(III) loaded cellulose nanocomposite bead (FeCNB) involves two different steps,
i) synthesis of cellulose nanobead (CNB) from cellulose powder and
ii) modification of CNB to Fe(III) loaded cellulose nanocomposite bead (FeCNB) by 10% ferric nitrate solution.

The sol-gel transformation of cellulose is the key step for the preparation of CNB. Cellulose, a repeated unit of anhydro glucose ring with chemical formula $(C_6H_{10}O_5)_n$ was used as the starting material of the adsorbent. The process involves dissolution, xanthation, syneresis and gelation of cellulose. At first, dissolution of cellulose powder was carried out in NaOH solution and after that, the solution yields a sol on xanthation and syneresis. The sol is then transformed to gel on further alkalization and shaking. In the last step, the gel is coagulated into a spherical bead in an aqueous methanolic solution. Shaking is preferred prior to ageing of the bead. The synthesis protocol of adsorbent is schematically represented in the following scheme (Figure 1).
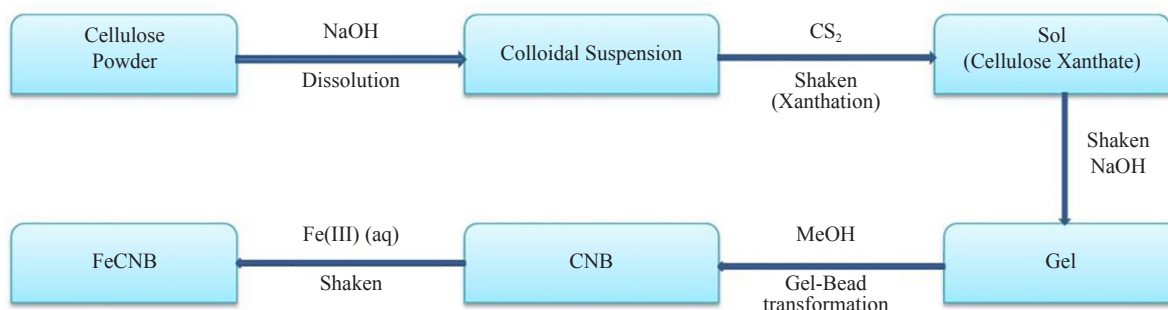
Figure 1. Synthesis protocol of Fe(III) loaded cellulose nanocomposite bead (FeCNB)

2.3 *Batch adsorption study*

Batch adsorption study of CR was carried out with 10 cm^3 of solution with a fixed dose of FeCNB, shaken in a 100 cm^3 conical flask until the process attained equilibrium. The study was performed with dye concentration ranging from 50 to 200 mgdm^{-3} at a controlled temperature. A visual representation of CR adsorption phenomenon on FeCNB is shown in Figure 2.

The initial pH of the solution was adjusted with either 0.1 M NaOH or 0.1 M HCl solution and the effect of pH was studied in the range from 3 to 10. Three different temperatures (293, 303 and 313 K) were chosen to study the effect of temperature on the adsorption process. The solute-adsorbent interaction time i.e., the contact time was varied from zero to 100 min. Adsorbent dose and shaking speed were varied from 0.5-2.5 gdm^{-3} and 50-150 spm respectively.

10 cm^3 of dye solution of different concentrations was shaken in a horizontal shaker with a fixed amount of

FeCNB and the final mixture was centrifuged for 5 min at 3500 rpm and the absorbance of the supernatant solution was measured (λ_{max}: 497 nm) using UV-VIS spectrophotometer (Shimadzu, UV-1800). Percent removal/retention or adsorption efficiency of the dye solution was measured by the following equation:

$$Removal(\%) = \frac{C_0 - C_e}{C_0} \times 100 \tag{1}$$

where, C_0 is the initial concentration and C_e is the equilibrium concentration (mgdm^{-3}) of dye solution.

Adsorption isotherm was investigated using dye with three different initial dye concentrations (50, 100 and 200 mgdm^{-3}) at three different temperatures. Thermodynamic parameters such as Gibbs free energy change, enthalpy change, and entropy change were also evaluated. The kinetic study was performed for each particular dye concentration at three different temperatures.
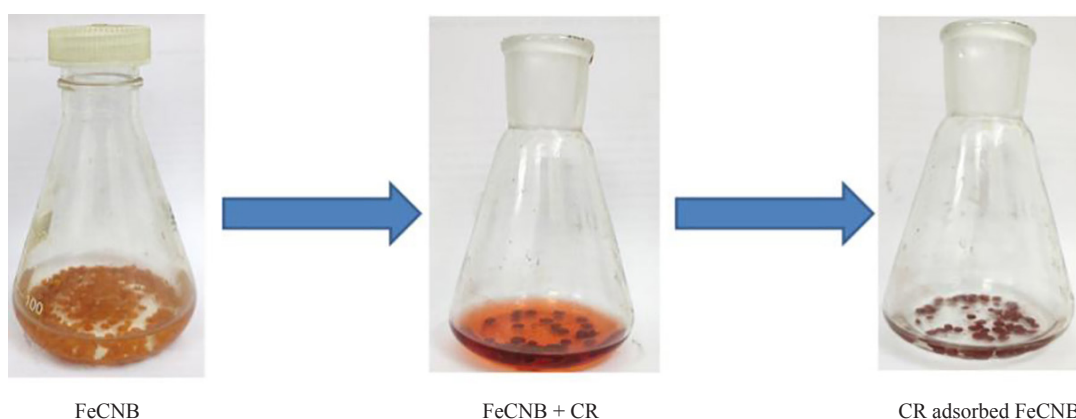
Figure 2. Visual representation of CR adsorption phenomenon on FeCNB

3. Result and discussion

3.1 *Characterization of the adsorbent*

The FT-IR spectra of the synthesized adsorbent in the solid state was investigated in the frequency range 400 to 4000 cm^{-1} (Perkin Elmer L120-000A IR spectrophotometer). The FTIR spectrum of FeCNB was compared with that of CNB to demonstrate any changes in the vibrational frequency of the functional group during loading of Fe(III) in FeCNB (Figure 3).

The broad band at 3403 cm^{-1} in CNB and 3412 cm^{-1} in FeCNB spectrum were due to the O-H stretching band of cellulose. Symmetrical C-H stretching band was appeared at 2919 cm^{-1} and 2917 cm^{-1} for CNB and FeCNB respectively. C-H bending (in plane) frequency of CNB and FeCNB appears at almost similar position (1372 cm^{-1} for CNB and 1373 cm^{-1} for FeCNB). The peaks corresponding to C-O-C, C-C-O, C-C-H deformation and stretching appeared at almost similar position (1372 cm^{-1} for CNB and 1373 cm^{-1} for FeCNB). Some new peaks in the range of 500-588 cm^{-1} were observed in FeCNB that were absent in the spectrum of CNB. These bands were due to the stretching and bending vibration of Fe-O and O-Fe-O respectively. It seems that Fe binds with the deprotonated hydroxyl groups of cellulose forming O-Fe-O or Fe-O bonds[18] resulting in little increase in the intensity of some peaks (3403, 1639, 2919, 1372, 1161, and 894 cm^{-1}) in Fe(III) modified CNB.

(a)

(b)
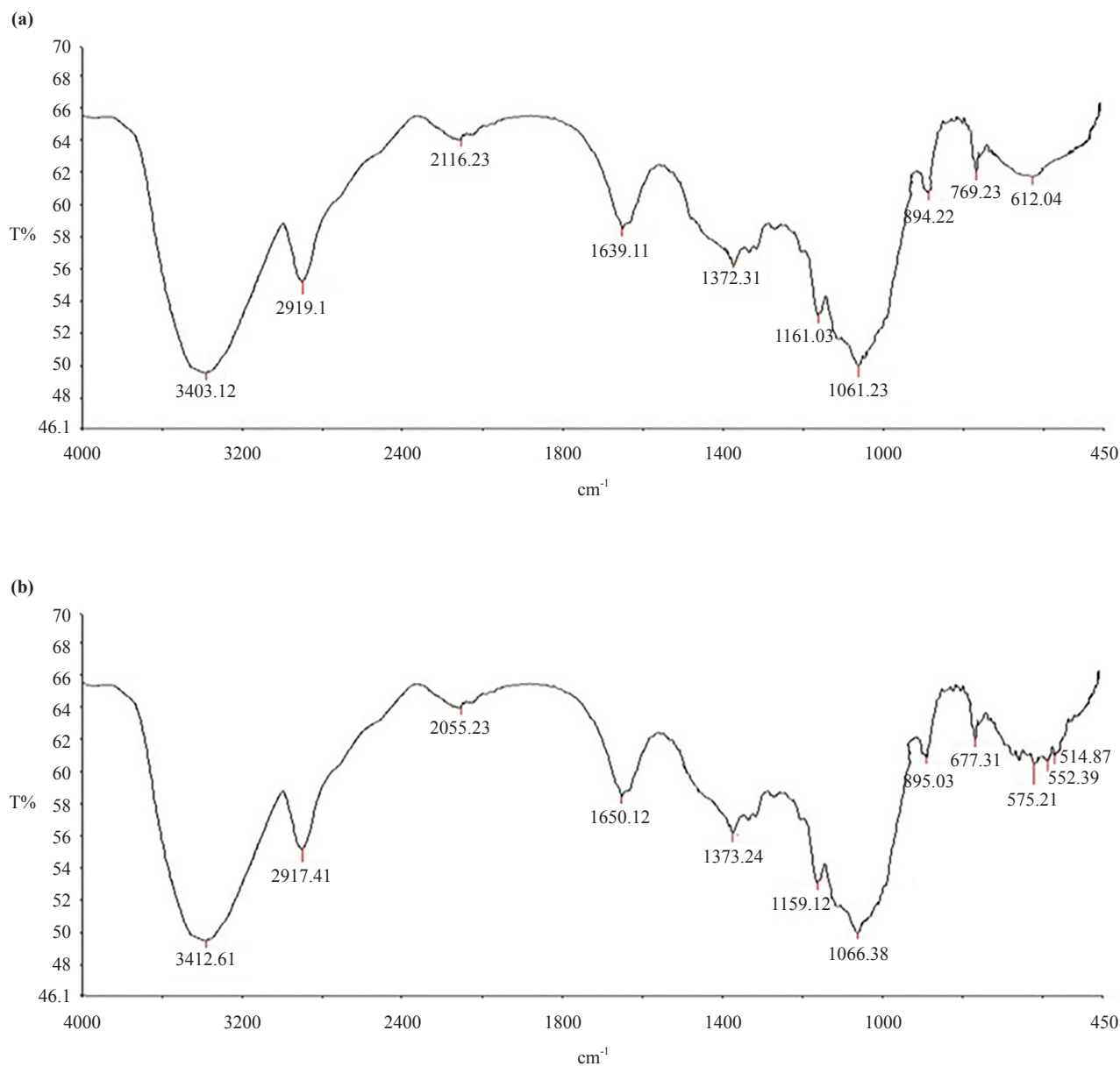
Figure 3. FT-IR spectra of (a) CNB), (b) Fe(III) loaded cellulose nanocomposite bead (FeCNB)

Zeiss scanning electron microscope (SEM: FEI Quanta FEG 250) was used to analyze high magnification images of the surface topography of FeCNB. FeCNB was dried in hot air oven for 6 h and the dried bead was coated with gold before loading to the SEM instrument. The sample was scanned with an electron beam with magnification of 162x and 1180x with a scale of 200 μm and 20 μm respectively. The presence of roughness of the surface of the adsorbent was confirmed from Figure 4. Further investigation on the particle size of FeCNB in the nanoscale at high magnifications was using FESEM study.
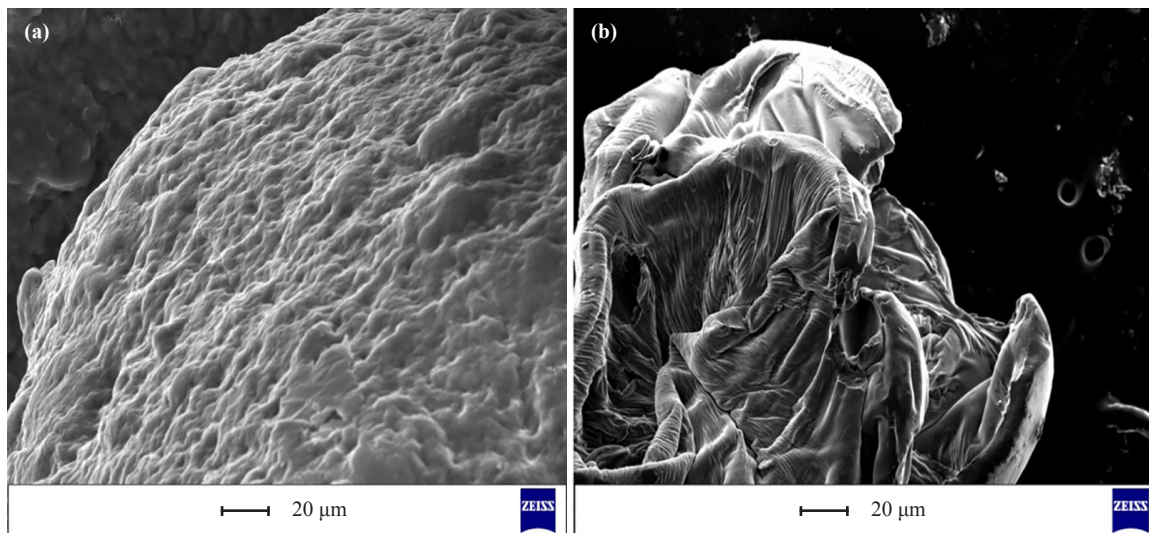
Figure 4. SEM images of FeCNB

Topographical analysis of FeCNB and CR adsorbed on FeCNB was performed using the FESEM (JEOL, JSM 6700 F with voltage 5.0 kV). Two different magnifications of 7000x and 30000x were selected with a scale of 1 µm and 100 nm for FeCNB (Figure 5). FESEM images revealed the nanocomposite nature with an average diameter of 21 nm for FeCNB.
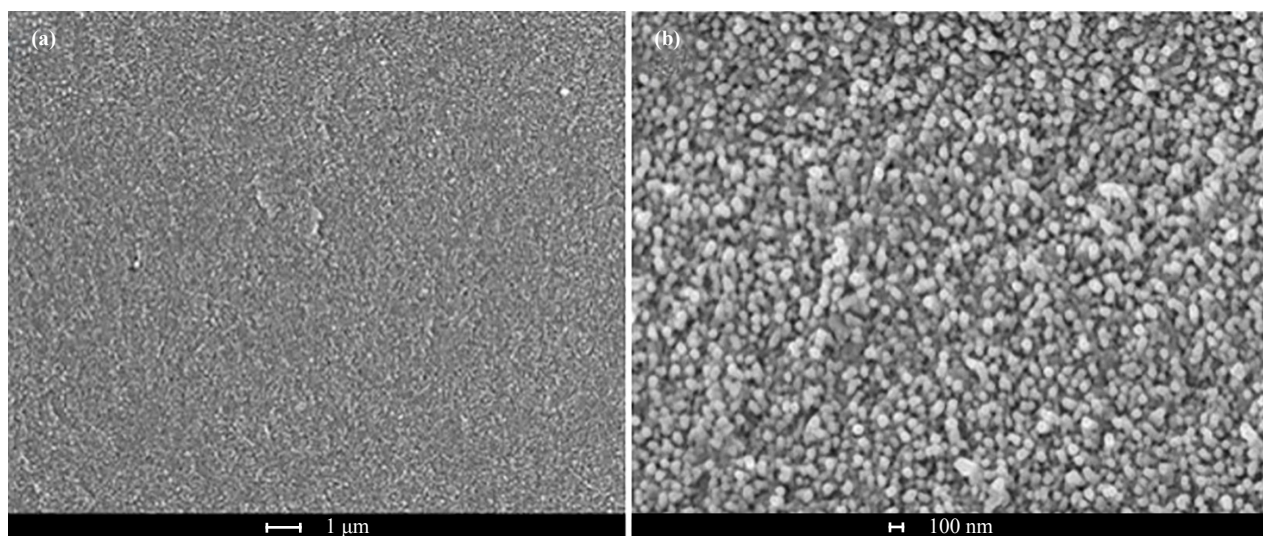
Figure 5. FESEM images of FeCNB

FESEM analysis of CR adsorbed on FeCNB was similarly performed at a similar environment and magnification scale as that of FeCNB (Figure 6). The nanocomposite nature of the adsorbent was found to remain unaltered after adsorption of CR. The average particle diameter was also found almost similar as that of FeCNB.
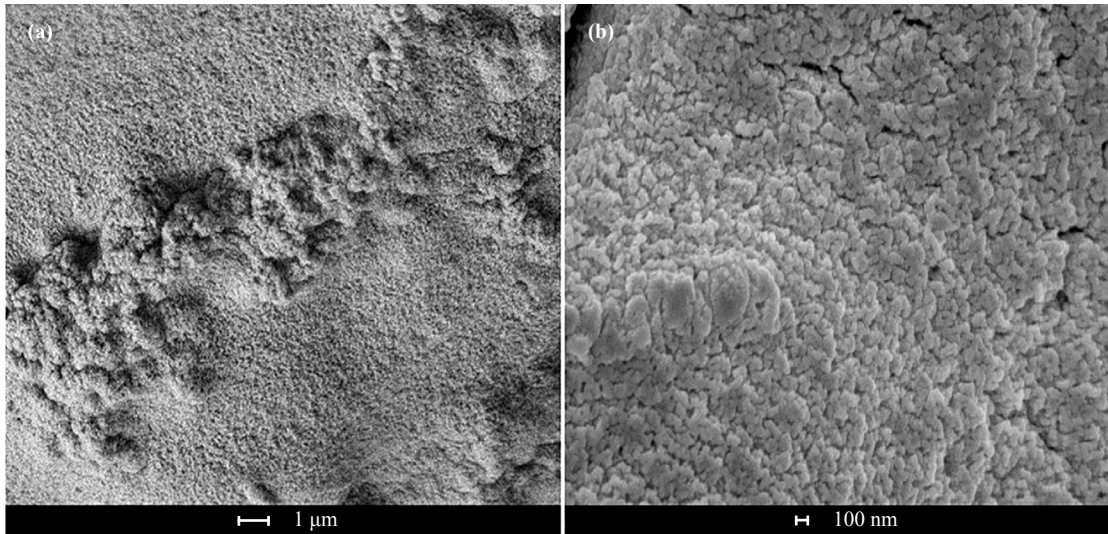
Figure 6. FESEM images of Congo red adsorbed on FeCNB

Energy dispersive X-ray analysis (EDAX) of Congo red loaded FeCNB was performed from the SEM instrument. EDAX spectrum of Congo red loaded FeCNB was represented in Figure 7. It confirms the presence of carbon, oxygen, iron, nitrogen, sulphur and sodium. The result of elemental analysis as weight percent (Wt %) and atomic percent (At %) are further presented in Table 2.
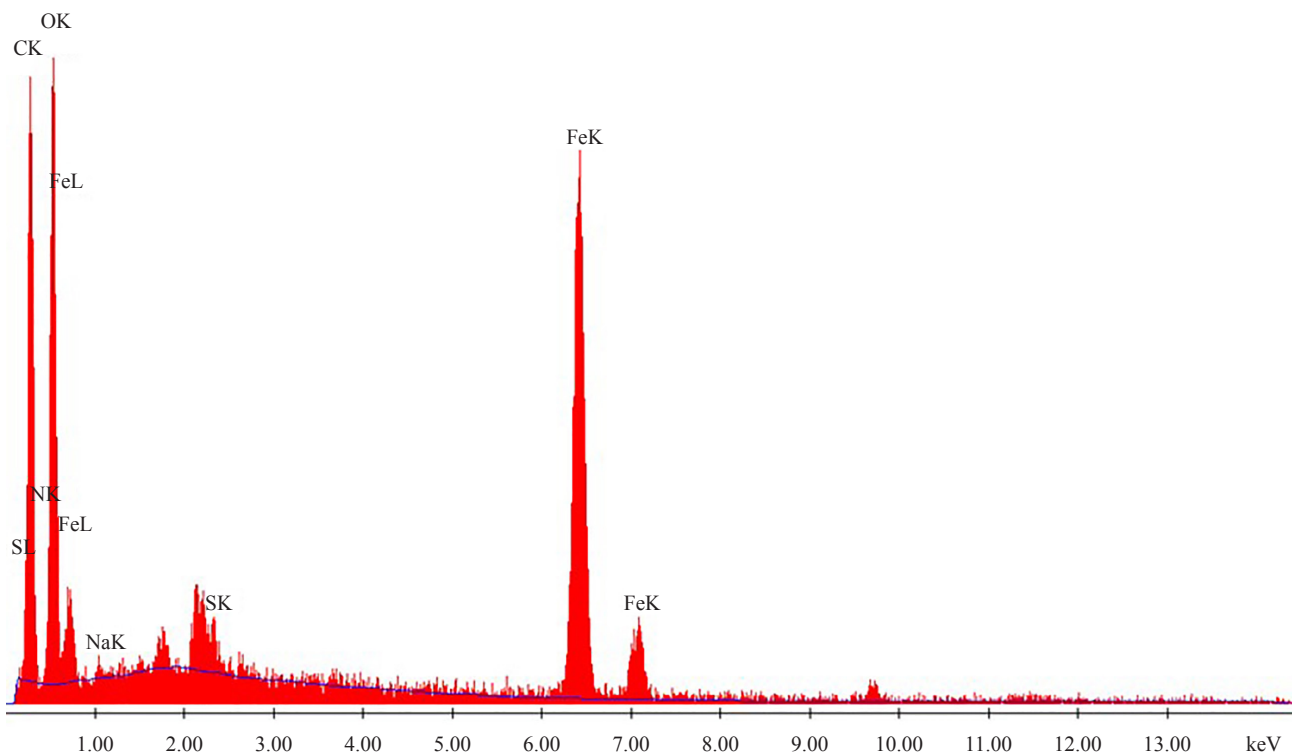
Figure 7. EDAX of Congo red adsorbed onFeCNB

Table 2. Elemental composition of Congo red adsorbed on FeCNB

Element	Wt %	Atomic percent (At %)
C(K)	46.74	61.06
N(K)	0.74	0.83
O(K)	32.96	32.33
Na(K)	0.43	0.29
S(K)	0.55	0.27
Fe(K)	18.59	5.22
Total	100.00	100.00

TEM analysis of synthesized FeCNB was carried out with the JEOL-JEM-2100-HR, to further investigate the nanoparticles below 20 nm. FeCNB was dispersed in DMSO by sonication for 360 min and the mixture was deposited immediately in a Cu grid coated with carbon. Excess mixture was soaked from the Cu grid using a tiny piece of filter paper and loaded to TEM for imaging.[19] The black spots in the TEM image (Figure 8) represent the nanoparticles of an average diameter of 5-10 nm.[20] The size distribution of particles in the nanoscale range is presented in the inset of Figure 8a.
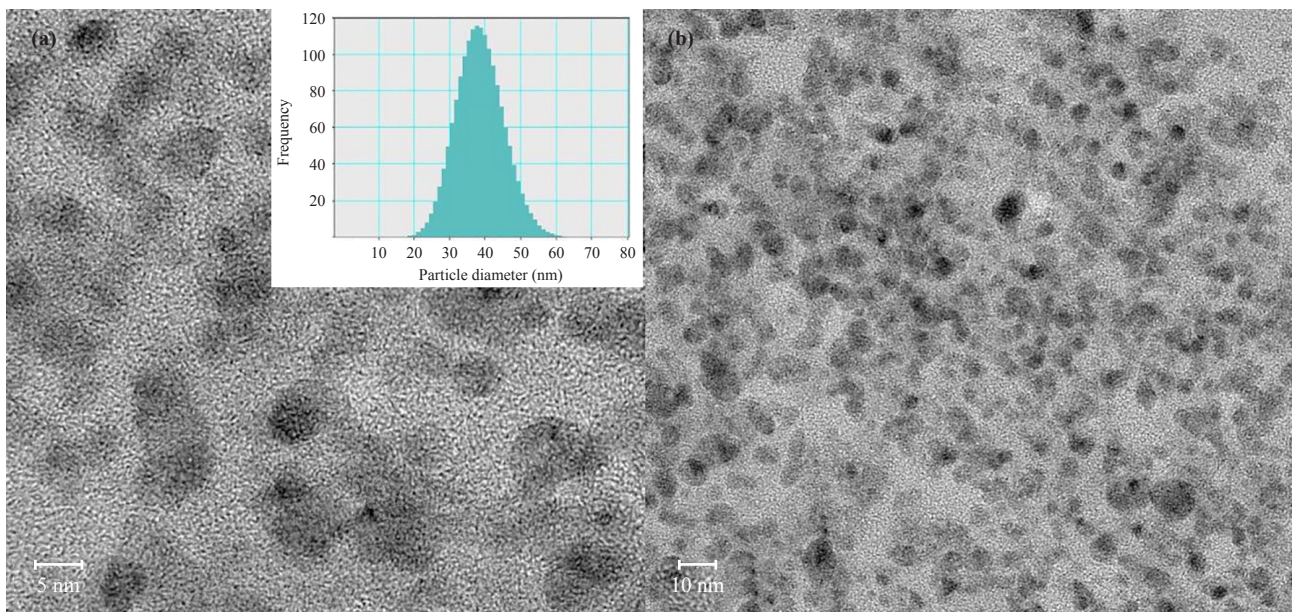
Figure 8. TEM images of FECNB (a) at 5 nm (b) at 10 nm scale

3.2 *Effect of operational parameters on Congo red removal*
3.2.1 *Effect of adsorbent dose*

The effect of adsorbent dose on CR removal using FeCNB was performed varying the FeCNB dose from 0.5 to 2.5 gdm^{-3}. Percent removal of the dye was increased initially with increasing adsorbent dose from 0.5 to 1.0 gdm^{-3}

and thereafter became almost constant. Figure 9(a) revealed the equilibrium adsorbent dose was 1.0 gdm^{-3} for dye concentration ranging from 50 to 200 mgdm^{-3}. With the adsorbent dose increase, the surface area as well as the active binding site increased and consequently the extent of adsorption also increased.[20] With further increase in adsorbent dose to 2.5 gdm^{-3}, the equilibrium removal percent was found to remain constant. Similar observation was reported by Sharma et al.[21]

3.2.2 *Effect of pH*

The initial solution pH is expected to have a considerable impact on removal efficiency of Congo red. The effect of pH was examined in Figure 9(b) keeping 90 min of contact time. The percent removal was increased from pH 2.0 to 6.0 and gradually decreased from pH 6.0 to 10.0. The point of zero charge (pH$_{ZPC}$) of FeCNB adsorbent being determined to be 7.58, the surface charge of FeCNB is expected to be positive at pH < 7.58. Thus, the electrostatic interaction between positive surface of FeCNB and the anionic dye molecules prevails leading to increased removal. Congo red is a typical dipole molecule with pK$_a$ value of 5.5. The anionic property of Congo red increases with pH, especially at pH > 5.5.[22] At low pH, both adsorbent surface and dye molecules are highly protonated due to high concentration and high ionic mobility of H$^+$ ions.[23] On increasing pH, extent of H$^+$ ions was decreased resulting in the increase in the percent removal of Congo red. At pH > 7.58, the surface of FeCNB became deprotonated and negatively charged environment increases due to presence of large amount of OH$^-$.[24] Consequently, the electrostatic repulsion between adsorbent surface and anionic dye molecules was increased with increasing pH and hence, the extent of adsorption was found to diminish rapidly at higher pH. An almost similar result was reported for Congo red removal by Roy and Mondal, 2017.[24]

3.2.3 *Effect of contact time*

The study of contact time, i.e., the interaction time between adsorbent surface and adsorbate molecules is one of the most important factors governing the adsorption equilibrium. The effect of contact time for adsorption of Congo red onto FeCNB bead was investigated by varying the contact time between 0-100 min at pH 6.0 for CR corresponding to three initial concentrations of 50, 100 and 200 mgdm^{-3} in Figure 9(c). It was found that the equilibrium reached in 90 min and further increase in contact time did not change the extent of adsorption. The percent removal was found to be 94.34 and 89.80% for the initial concentration of 50 and 200 mgdm^{-3}, respectively. A high removal rate, at the start, was found for each solution concentration because of the accessibility of more active/binding sites on FeCNB. With progress of adsorption, the active sites of the adsorbent surface became gradually exhausted by the dye molecules leading to a slow extent of percent removal. On reaching the equilibrium, no appreciable change of percent removal was observed. The equilibrium was mainly attained due to saturation of active or binding sites of the adsorbent surface.

3.2.4 *Effect of shaking speed*

The effect of shaking speed on removal of Congo red using 1.0 mgdm^{-3} of FeCNB at pH 6.0 was investigated by varying shaking speed from 50 to 150 spm by a horizontal shaking machine. With increase in shaking speed from 50 to 100 spm, percent removal was increased from 51.44 to 89.61% corresponding to dye solution of 200 mgdm^{-3}, and from 65.04 to 94.23% corresponding to dye solution of 50 mgdm^{-3} (Figure 9d). It may be assumed that the higher shaking speed increases the collision between dye molecules and adsorbent surface, resulting in a faster dye-adsorbent interaction. The extent of adsorption remained almost same beyond the shaking speed of 150 spm for dye solution of different concentrations.[25]

3.2.5 *Effect of initial dye concentration*

During the process of adsorption, the most important driving force between liquid and solid phases is certainly the initial dye concentration. The effect of initial dye concentrations on percent removal of Congo red was investigated using 1.0 gdm^{-3} of FeCNB at pH 6.0. Figure 9(e) demonstrated that the percent removal was decreased from 94.23 to 89.61% with an increase in initial dye concentration from 50 to 200 mgdm^{-3} at 303 K. This is probably due to the limited number active sites on the adsorbent surface. At low concentrations, all the dye molecules could find the active site on adsorbent surface resulting almost complete removal of dye molecules by FeCNB. At higher concentrations, all the dye

Fine Chemical Engineering

molecules could not adhere to this limited number of active sites resultingin sharp decrease in percent removal.[26]

3.2.6 *Effect of temperature*
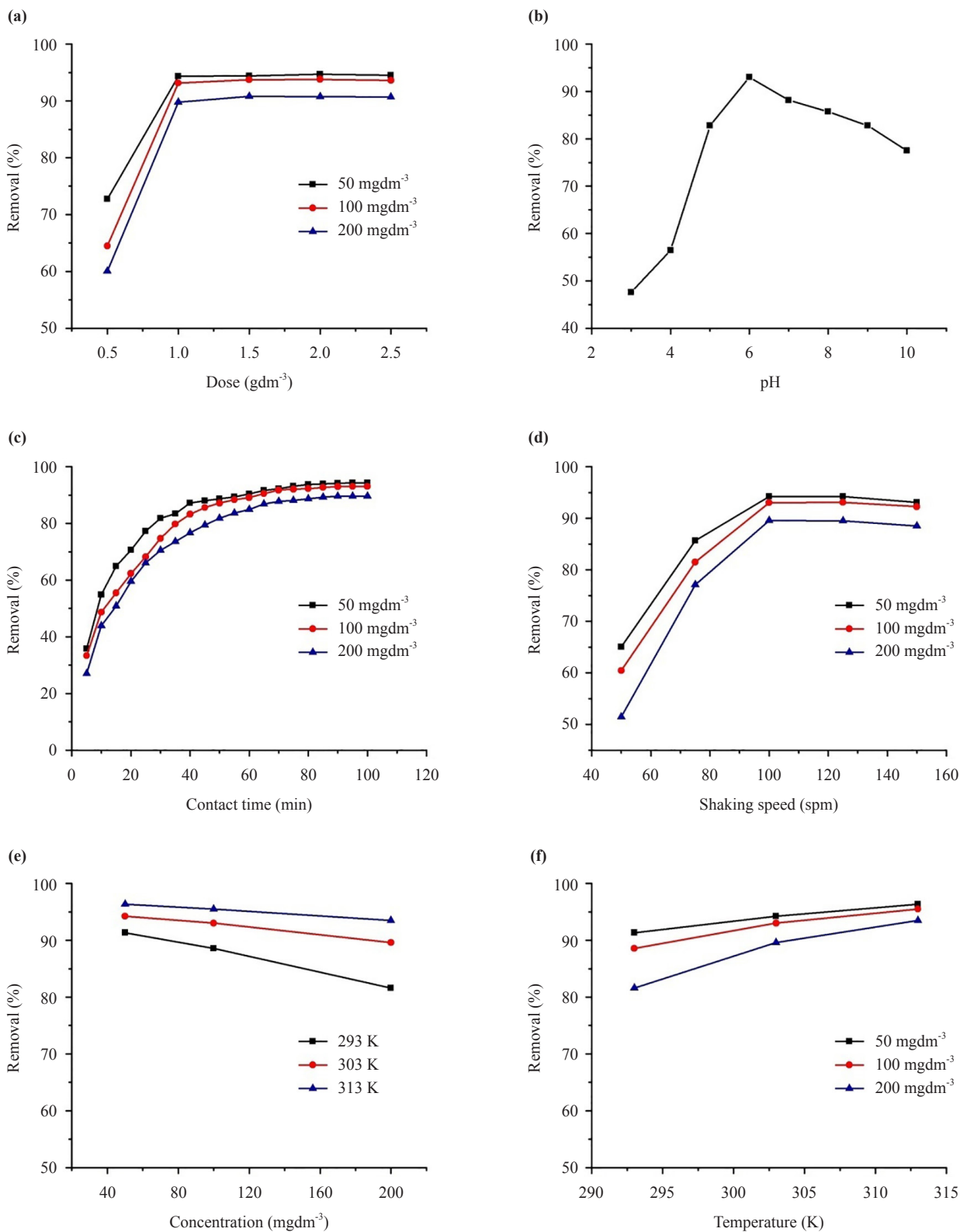
Figure 9. Effect of a) adsorbent dose, b) pH, c) contact time, d) shaking speed, e) concentration and f) temperature on CR removal

The effect of temperature on CR adsorption was investigated by varying the temperature from 293 to 313 K for three different CR concentrations and keeping all other variables at optimum conditions. The percent removal of CR was found to increase with temperature (Figure 9f) implying that the process is endothermic in nature. As the temperature increased from 293 to 313 K, the amount of adsorption was found to increase from 0.46 to 0.48 mgg^{-1}, 0.88 to 0.95 mgg^{-1} and 1.63 to 1.87 mgg^{-1} corresponding to CR concentrations of 50, 100 and 200 mgdm^{-3} respectively.

3.3 *Adsorption isotherm study*

Study of the adsorption isotherm reveals the feasibility criterion of the adsorption process. The isotherm models tested are: i) two-parameters viz. Langmuir, Freundlich, Temkin and Dubinin-Radushkevichand ii) three-parameters viz. Sips in order to find out the most suitable model predicting the CR-FeCNB interaction.

3.3.1 *Langmuir isotherm model*

The Langmuir model in the linear form is expressed as[27],

$$\frac{C_e}{q_e} = \frac{1}{q_m K_L} + \frac{C_e}{q_m} \tag{2}$$

where, C_e (mgdm^{-3}) is the equilibrium CR concentration in solution, q_e (mgg^{-1}) represents the amount of CR adsorbed on FeCNB. The Langmuir constant K_L (dm^{3}mg^{-1}) is related to adsorption energy and q_m (mgg^{-1}) is the maximum adsorption capacity.

Figure 10(a) represents the linear plot of $\frac{C_e}{q_e}$ against C_e at three different temperatures viz., 293, 303 and 313 K. The values of q_m and K_L were determined from slope and intercept (Table 3). It was found that the regression coefficient (R^2) values were more than 0.99 for CR at all the three temperatures. It was also found that the values of Langmuir isotherm constants i.e., q_m and K_L were found to increase with temperature. The maximum adsorption capacity of FeCNB was found to increase from 2.52 to 3.59 mgg^{-1} for temperature increase from 293 to 313 K.

(c)

(d)

(e)
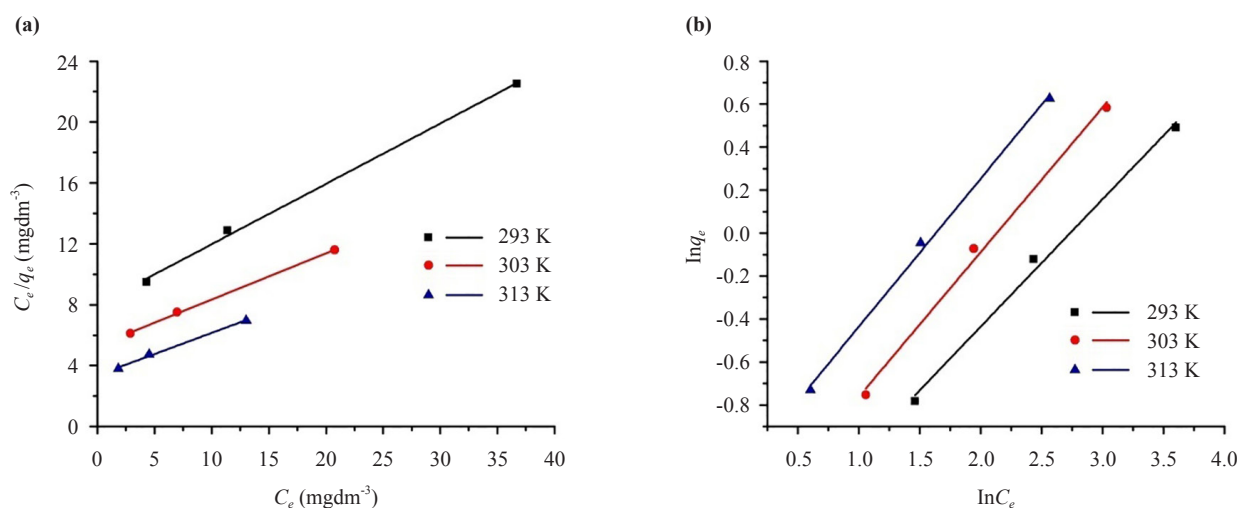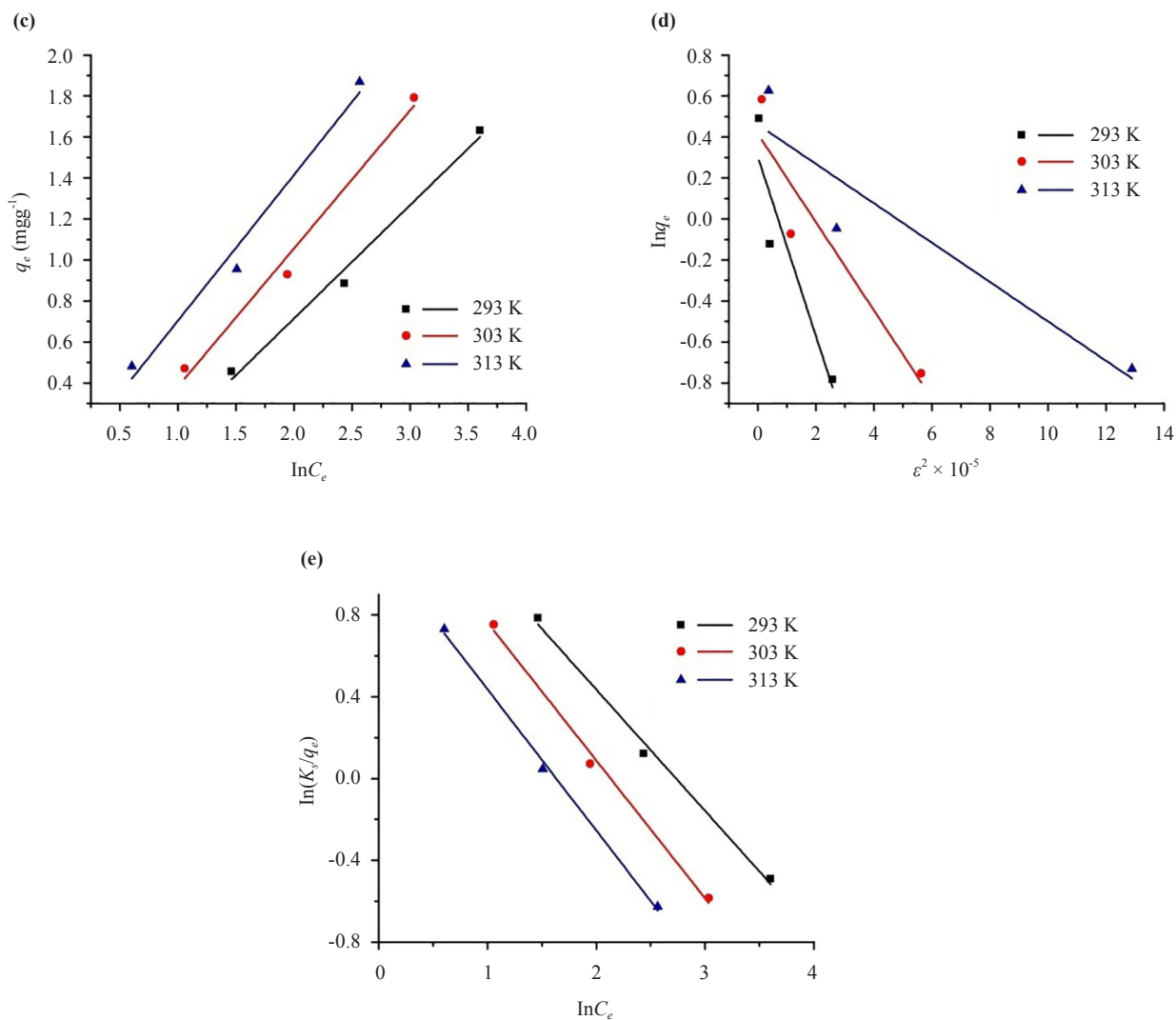
Figure 10. Plot of a) Langmuir, b) Freundlich, c) Temkin, d) Dubinin-Radushkevich e) Sips isotherm model

Weber and Chakraborty[28] described the characteristics of adsorption of adsorbate molecules by a dimensionless constant, the separation factor (R_L), to describe the feasibility of adsorption process. R_L can be expressed as:

$$R_L = \frac{1}{1 + K_L C_0} \tag{3}$$

where, K_L is the Langmuir constant and C_0 is the initial dye concentration. R_L value may reveal the characteristics of adsorption process[29] as,

feasible, when $0 < R_L < 1$;
linear when $R_L = 1$;
unfavourable, when $R_L > 1$ and
irreversible, when $R_L = 0$.

The R_L value of CR adsorption at three different temperatures (293, 303 and 313 K) and three different concentrations (50, 100 and 200 mgdm^{-3}) were represented in Figure 11(a) and Figure 11(b) respectively. The feasibility of CR adsorption on FeCNB was confirmed from the values of R_L as all the values were found to lie between 0 and 1.

The R_L value was found to decrease with increase in concentration at each temperature (Figure 11a) and decrease with increase in temperature at each concentration (Figure 11b).
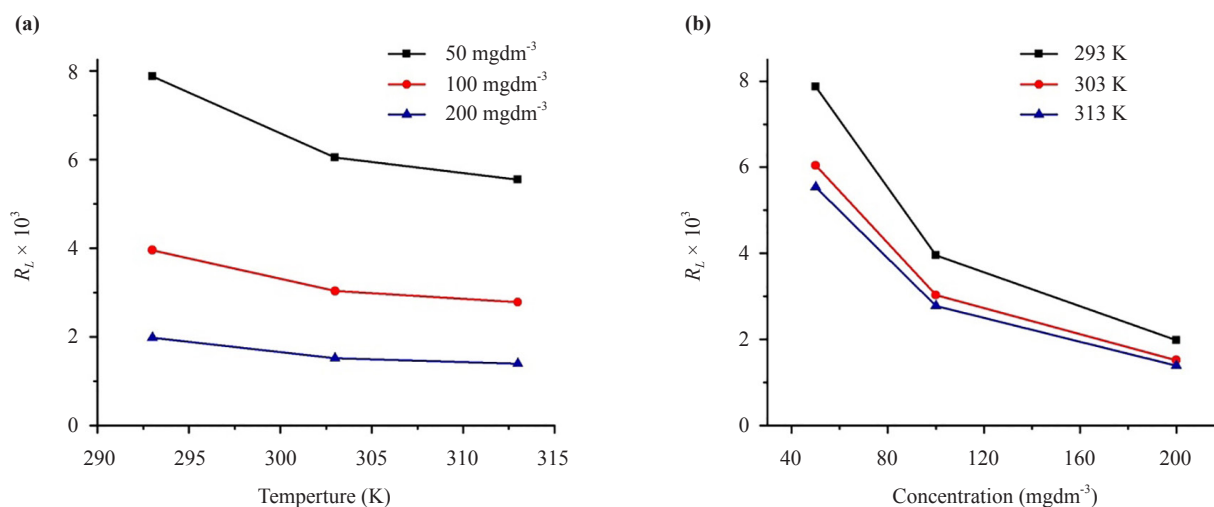
Figure 11. Variation of separation factor (R_L) with (a) temperature (b) concentration

Therefore, it can be concluded that the adsorption of CR on FeCNB is favourable at the experimental concentration and temperature range.

3.3.2 *Freundlich isotherm model*

Freundlich isotherm equation is applicable for adsorption of solute on heterogeneous surfaces. Exponential distribution of solute molecules, their energies and heterogeneity of surface of adsorbent are well described by Freundlich equation.[30]

The linear form of Freundlich isotherm can be represented as:

$$\ln q_e = \ln K_F + \frac{1}{n}\ln C_e \tag{4}$$

where, C_e (mgdm^{-3}) is the equilibrium concentration of adsorbate in solution, q_e (mgg^{-1}) represents the amount of solute adsorbed on adsorbent. The Freundlich constants $1/n$ and K_F (gmg^{-1}) (mgdm^{-3})$^{-1/n}$ express the intensity and the capacity of adsorption respectively. The value of $1/n$ confirms the feasibility of a particular adsorption process. The adsorption process is considered to be favourable when $0 < 1/n < 1$, irreversible when $1/n = 0$ and unfavourable when $1/n > 1$.[31]

Figure 10(b) represented the linear plot of $\ln q_e$ against $\ln C_e$ of CR adsorption. Freundlich constants $1/n$ and K_F were calculated from slope and intercept respectively. All $1/n$ values of CR adsorption at different temperatures are found to lie between 0 and 1 suggesting favourable nature of the adsorption processes for CR at the studied concentration and temperature range. K_F values are found to increase from 19.77 to 32.46 gmg^{-1} with increase in temperature from 293 to 313 K (Table 3). Higher R^2 values of the plot suggest the good fitting of the model within the studied temperature range.

3.3.3 *Temkin isotherm model*

Temkin isotherm model describes the indirect effect of adsorbent-adsorbate interaction in adsorption process. The most important assumption is that the heat of adsorption of a particular adsorption process decreases linearly rather than logarithmic, with increase of surface coverage.[31] This model is valid for a moderate concentration of adsorbate in

solution. Temkin isotherm in linear form can be expressed as,

$$q_e = \left(\frac{RT}{B_{Tem}}\right)\ln A_{Tem} + \left(\frac{RT}{B_{Tem}}\right)\ln C_e \tag{5}$$

where, q_e and C_e represent the usual meaning. R is the universal gas constant, $T(K)$ is the temperature at which the adsorption process is performed. A_{Tem} (dm^3mg^{-1}) and B_{Tem} ($Jgmg^{-1}mol^{-1}$) represent the adsorption capacity and the heat of adsorption respectively.

The Temkin isotherm model plot for CR was represented in Figure 10(c). Temkin isotherm constants B_{Tem} and A_{Tem} were calculated from slope and intercept respectively. With increase in temperature, A_{Tem} is found to increase from 0.494 to 1.010 dm^3mg^{-1} while B_{Tem} is found to decrease from 4409 to 3657 $Jgmg^{-1}mol^{-1}$ (Table 3).

3.3.4 *Dubinin-Radushkevich isotherm model*

Dubinin-Radushkevich isotherm model, applicable for moderate solute concentrations in solution, is generally used to ascertain the mechanism with Gaussian energy distribution for solute adsorption onto heterogeneous surface.[30] The isotherm model can be expressed as[32]

$$\ln q_e = \ln q_{DR} - K_{ad}\varepsilon^2 \tag{6}$$

where, ε known as Polanyi potential[32], is expressed as,

$$\varepsilon = RT\ln(1+\frac{1}{C_e}) \tag{7}$$

where, all the terms bear their usual meanings.

The values of K_{ad} and q_{DR} (Table 3) were determined from the slope and intercept respectively from the plot of $\ln q_e$ against ε^2 (Figure 10d). q_{DR} was found to increase from 1.354 to 1.585 with increase in temperature from 293 to 313 K while the K_{ad} value decreased from 0.436 to 0.096 with rise in temperature (Table 3).

3.3.5 *Sips isotherm model*

Sips isotherm model, considered as a combination of Langmuir and Freundlich isotherm model can be expressed in linear form as,

$$\ln\left(\frac{K_s}{q_e}\right) = -\beta_s \ln C_e + \ln(A_s) \tag{8}$$

where, K_s (gdm^{-3}) and A_s (dm^3mg^{-1}) are the Sips isotherm constants, β_s is the Sips isotherm model exponent. At low solute concentration, the model reduces to Freundlich model whereas at high solute concentration, the model turns into Langmuir model.[33]

A linear plot of $\ln(K_s/q_e)$ against $\ln C_e$ (Figure 10e) was made for all studied temperatures. It was observed that the values of A_s decreased from 5.05 to 3.08 dm^3mg^{-1} with increase in temperature from 293 to 313 K. On the other hand, the values of β_s are found to be increase from 0.593 to 0.689 with rise in temperature from 293 to 313 K in the present case (Table 3).

Table 3. Isotherm parameters in batch operation of CR

Isotherm	T (K)	q_m (mgg^{-1})	$K_L \times 10^2$ (dm^{3}mg^{-1})	R^2
Langmuir	293	2.52	4.95	0.9973
	303	3.29	5.73	0.9992
	313	3.59	8.27	0.9961
Freundlich	T (K)	$K_F \times 10^2$ (gmg^{-1}) (mgdm^{-3})$^{-1/n}$	$1/n$	R^2
	293	19.77	0.5928	0.9944
	303	23.81	0.6733	0.9951
	313	32.46	0.6893	0.9972
Temkin	T (K)	A_{Tem} (dm^{3}mg^{-1})	B_{Tem} (Jgmg^{-1}mol^{-1})	R^2
	293	0.494	4409	0.9890
	303	0.999	3741	0.9876
	313	1.010	3657	0.9816
Dubinin-Radushkevich	T (K)	K_{ad}	q_{DR}	R^2
	293	0.436	1.354	0.8744
	303	0.215	1.514	0.8876
	313	0.096	1.585	0.8877
Sips	T (K)	β_s	A_s (dm^{3}mg^{-1})	R^2
	293	0.593	5.05	0.8992
	303	0.673	4.20	0.9944
	313	0.689	3.08	0.9847

3.4 *Kinetic study*

In order to determine the rate of adsorption and plausible mechanism of CR-FeCNB interaction, three different kinetic models viz. pseudo-first-order, pseudo-second order and Weber-Morris intraparticle diffusion model, have been studied.

3.4.1 *Pseudo first order (Lagergren) rate equation*

In pseudo-first-order (PFO) model[34], adsorption of solute particles on the surface of a particular adsorbent obeys

the following first order expression, also known as Lagergren rate equation, as,

$$\ln(q_e - q_t) = \ln q_e - k_1 t \qquad (9)$$

where, q_t (mgg^{-1}) is the amount of solute adsorbed onto adsorbent surface at time t, k_1 is the rate constant per min and q_e (mgg^{-1}) is equilibrium adsorption capacity. A plot of $\ln(q_e - q_t)$ against t yielded k_1 (Table 4) from the slope in Figure 12(a). The rate constant k_1 is found to increase from be 5.65×10^{-2} to 6.10×10^{-2} for the initial dye concentration range 50 to 200 mgdm^{-3} but not following a definite trend (Table 4). The regression coefficient (R^2) values are comparatively lower (< 0.979).

Table 4. Kinetic parameters of CR adsorption

Model	Conc. (mgdm^{-3})	$K_1 \times 10^2$ (min^{-1})	R^2	
Pseudo 1st order	50	5.65	0.9643	
	100	6×10	0.9793	
	200	5.84	0.9591	
Pseudo 2nd order	Conc. (mgdm^{-3})	$K_2 \times 10^2$ (gmg^{-1}min^{-1})	R^2	
	50	21.83	0.9993	
	100	7.44	0.9983	
	200	3.21	0.9992	
Weber-Morris and Arrhenius	Conc. (mgdm^{-3})	$K_{id} \times 10^2$ (gmg^{-1}min$^{-1/2}$)	Intercept. 10^2	E_a (kJmol^{-1})
	50	0.65	41.0	4.273
	100	1.14	82.14	
	200	3.51	145.9	

3.4.2 *Pseudo-second-order rate equation*

A pseudo-second-order (PSO) model assumes that the rate of adsorption depends on the amount of solute and the available active sites present on adsorbent surface. A typical second order equation can be expressed as[34]:

$$\frac{t}{q_t} = \frac{1}{k_2 q_e^2} + \frac{t}{q_e} \qquad (10)$$

where, k_2 is pseudo second order rate constant.

A plot of $\dfrac{t}{q_t}$ against time t at a constant temperature was presented in Figure 12(b). The value of k_2 (gmg^{-1}min^{-1}) was evaluated from the intercept of the plot. The values of k_2 are found decrease from 21.83×10^{-2} to 3.21×10^{-2} gmg^{-1}min^{-1} following a definite trend for the initial dye concentration range of 50 to 200 mgdm^{-3} (Table 4). The regression coefficient (R^2) values are comparatively higher (> 0.998). Comparing the values of R^2, it is indicated that the PSO

model is the most suitable than PFO for Congo red adsorption onto FeCNB within the studied concentration range.

3.4.3 *Weber and Morris rate equation*

The adsorption process, being a complex one, involves the mass transfer of the solute, as well as surface and pore diffusion of the solute over the adsorbent.[35]

The rapid adsorption at the beginning of the process is considered as the surface diffusion and next is the pore or the intra-particle diffusion, which is a slow process. The Weber and Morris equation, the commonly known equation of intra-particle diffusion model is expressed as follows:

$$q_t = k_{id}t^{\frac{1}{2}} + C \tag{11}$$

where (mg g^{-1}min$^{-1/2}$) is the intra-particle diffusion constant or the rate constant for pore diffusion. A plot of q_t against square root of t was made (Figure 12c) to show two distinct regions indicating the involvement of two different steps in adsorption of CR molecules on FeCNB. The initial curved portion is due to external film diffusion which is the diffusion of CR molecules from bulk solution to the surface of FeCNB. The second portion is a linear portion that indicates the intra-particle diffusion of CR molecules into the adsorbent; the rate constant of which was evaluated from the slope. The characteristic kinetic parameters of intra-particle diffusion of Congo red are represented in Table 4.

3.4.4 *Arrhenius equation*

The activation energy of pore diffusion was determined using the Arrhenius equation[36] expressed as:

$$\ln k_{id} = \ln A - \frac{E_a}{RT} \tag{12}$$

where, A is the pre-exponential factor, K_{id} is the diffusion constant, E_a is the activation energy, and R is the universal gas constant. A plot of $\ln K_{id}$ against 1/T yielded E_a of the process from the slope (Figure 12d).
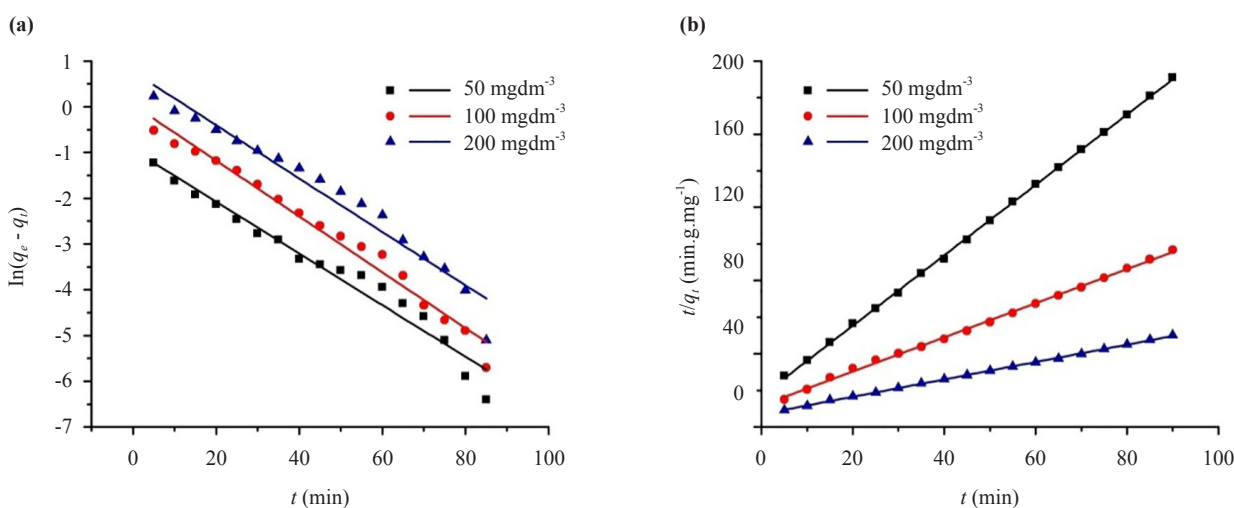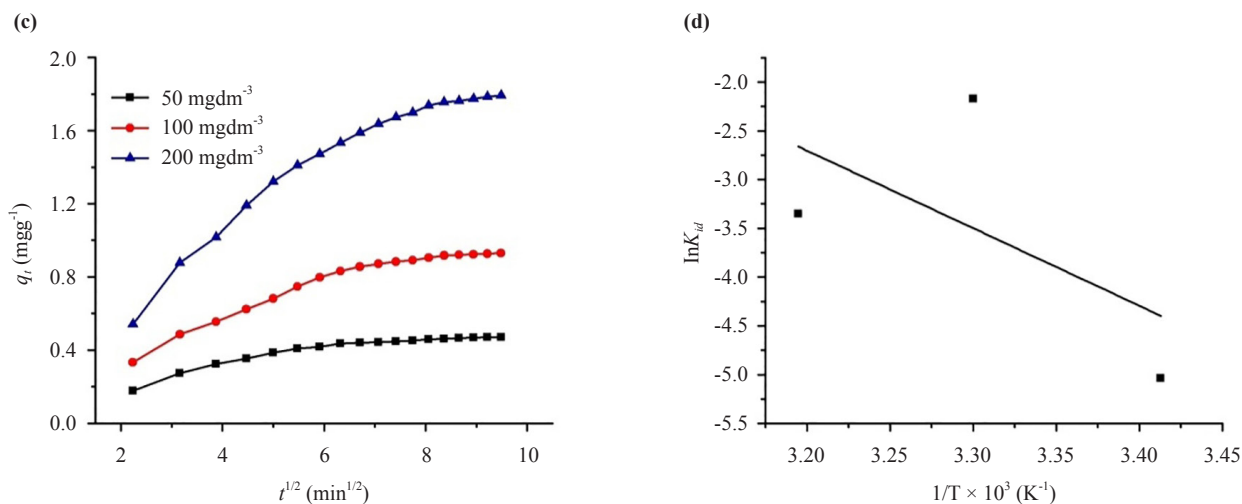
Figure 12. Plot of a) pseudo first-order, b) pseudo-second-order and c) Weber and Morris d) Arrhenius equation

3.5 *Thermodynamics of CR adsorption*

Thermodynamic behavior of the adsorption of CR onto FeCNB was determined from the thermodynamic parameters such as the change in Gibb's free energy (ΔG^0), entropy (ΔS^0) and enthalpy (ΔH^0). The Gibb's free energy is correlated with the equilibrium constant (K_c) at a temperature T, as,

$$\Delta G^0 = -RT \ln K_C \qquad (13)$$

The change in enthalpy (ΔH^0) and change in entropy (ΔS^0) was evaluated from van't Hoff equation as,

$$R \ln K_C = \Delta S^0 - \frac{\Delta H^0}{T} \qquad (14)$$
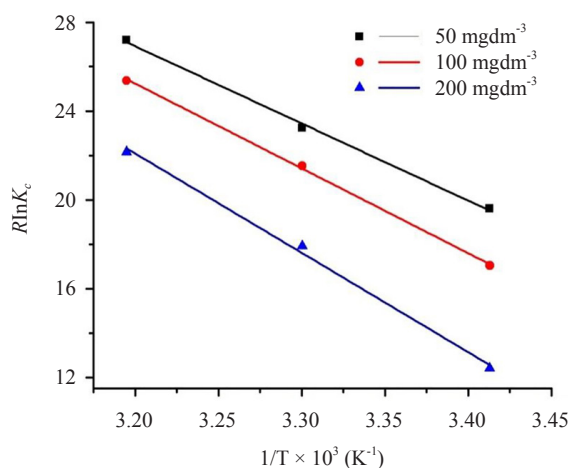
Figure 13. Plot of van't Hoff equation

A plot of $R\ln K_c$ against 1/T yields a straight line (Figure 13) and the values of ΔH^0 and ΔS^0 were evaluated from slope and intercept respectively (Table 5)

Table 5. Thermodynamic parameters of CR adsorption

Conc. (mgdm^{-3})	T(K)	$-\Delta G^0$ (kJmol^{-1})	ΔH^0 (kJmol^{-1})	ΔS^0 (Jmol^{-1}K^{-1})
50	293	5.64	34.79	0.138
	303	7.02		
	313	8.40		
100	293	4.85	38.22	0.147
	303	6.32		
	313	7.79		
200	293	3.85	44.76	0.165
	303	5.23		
	313	6.88		

3.6 *Desorption study*

The acceptability of an adsorption method depends not only on the efficiency of the adsorbent, but also on the reusability of the adsorbent. Desorption study of FeCNB was performed using acid (HCl), alkali (NaOH) and alcohol (methanol and ethanol). It was found that 0.1 M NaOH was most suitable eluting agent for desorption of CR from the adsorbed phase (Figure 14a). In order to study the capacity of the adsorbent for repetitive use successive removal-desorption operations were performed. Moreover, the stability versus efficiency of FeCNB with different retention/removal-desorption cycles was investigated using NaOH of different strengths viz. 0.05 M, 0.1 M and 0.5 M (Figure 14b).
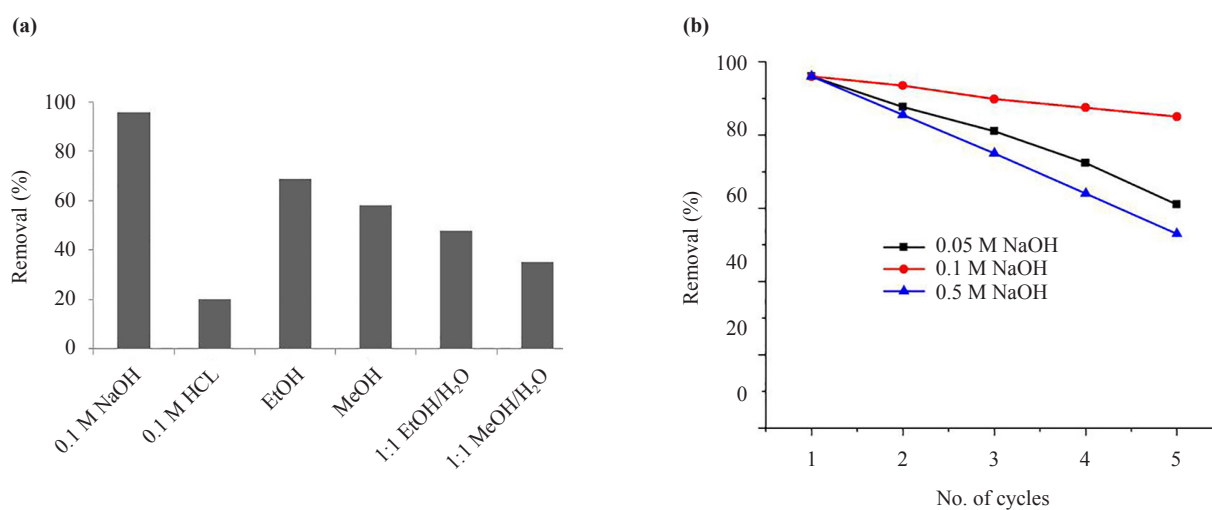
Figure 14. (a) Desorption of Congo red b) Efficiency for repeated use

With progress of removal-desorption cycles, the removal decreases slightly using 0.1 M NaOH, but steadily with 0.05 M NaOH and sharply with 0.5 M NaOH, up to five cycles. The steady decrease using 0.05 M NaOH was due to insufficient elution of the dye, while sharp decrease using 0.5 M NaOH was due to stability loss of FeCNB.After five successive operations, Congo red removal was found to decrease rapidly from 96 to 53% at higher strength of NaOH (0.5 M) and also was found to decrease rapidly from 96 to 61% at 0.05 moldm^{-3} NaOH as an eluent. On the other hand, a slow decrease in percent removal from 96 to 85 % was observed using 0.1 M NaOH as an eluent. Thus, 0.1 M NaOH is employed as the most suitable eluent.

3.7 *Comparison of FeCNB with similar adsorbents*

The adsorption characteristics of FeCNBis compared with some recently reported adsorbents[26, 37-43] in Table 6. FeCNB was found to remove 89.6% of Congo red from the aqueous solution at an initial concentration of 200 mgdm^{-3} at 303 K. Except PANI@ZnO[37] nanocomposite and Pb-FeONPs[38], the other adsorbents are dealing with lower dye concentration. FeCNB efficiency in removing CR is found somewhat comparable, in some situations is even better. Moreover, the adsorbent synthesis is simple, the precursor is nature derived and easily available.

Table 6. Adsorption of CR over different reported adsorbents

Sl. No	Adsorbent	Dose (g)	pH	Conc. (mgdm^{-3})	Contact time (min)	Temp. (K)	Removal (%)	Reference
1	PANI@ZnO nanocomposite	0.010	5.0	150	60	298	76.48	[37]
2	Pb$_{0.06}$Fe$_{0.7}$O$_3$ nanoparticles (Pb-FeONPs)	0.200	6.5	200	40	-	94.42	[38]
3	HDTMABr	3.0*	7.0	60	90	297	99.24	[39]
4	HCl-modified wood charcoal	2.0*	3	20	400	298	98	[26]
5	NH$_3$-modified wood charcoal	2.0*	3	20	400	298	80	[26]
6	Unmodified wood charcoal	2.0*	3	20	400	318	87	[26]
7	Activated Moringa oleifera seed coat	0.1	7.4	10	90	-	> 90%	[40]
8	Chemically modified rice husk char (CMRHC)	0.5	7	80	20	303	96.6	[40]
9	Rice husk(RH)	0.5	7	80	20	303	81.3	[41]
10	Fe$_3$O$_4$/magnetic grape fruit peel	0.05	-	50	10		92.88	[42]
11	Pomegranate seeds wastes	0.2	7	25	80	298	60	[43]
12	FeCNB	1.0*	6.0	50	90	303	94.2	Present study
13	FeCNB	1.0*	6.0	100	90	303	93.0	Present study
14	FeCNB	1.0*	6.0	200	90	303	89.6	Present study

*gdm^{-3}

4. Conclusion

Fe(III) impregnated cellulose nanocomposite bead (FeCNB) was found to be an efficient adsorbent for the

remediation of Congo red from aqueous solutions. The extent of adsorption increased with increase in pH and highest percent removal was achieved at pH of 6.0. The percent removal of Congo red was increased with increase in contact time, shaking speed, adsorbent dose and temperature. Experimental data fitted best to Langmuir isotherm model and the kinetic study suggested that the process followed pseudo-second order indicating that the rate of adsorption was dependent on both concentration of CR solution and FeCNB dosage. Spontaneity and endothermic nature of the process were affirmed by the negative Gibbs free energy(ΔG^0) and positive enthalpy (ΔH^0)and entropy (ΔS^0) respectively. Desorption of the adsorbed CR was investigated with acid, alkali and alcohols, indicating alkali as the suitable desorption agent. Moreover, the stability of the adsorbent and efficiency of FeCNB was retained up to five adsorption-desorption cycles using 0.1 M NaOH.

Acknowledgements

Conflict of interest

The authors declare that they have no conflict of interest.

Ethical approval

All ethical guidelines have been adhered.

References

[1] Kumar, A.; Dixit, U.; Singh, K.; Gupta, S. P.; Beg, M. S. J. Structure and properties of dyes and Pigments. In *Dyes and Pigments-Novel Applications and Waste Treatment*; Papadakis R., Ed.; IntechOpen, 2021; pp 131.

[2] Aksakal, O.; Ucun, H. Equilibrium, kinetic and thermodynamic studies of the biosorption of textile dye (Reactive Red 195) onto Pinus sylvestris L. *J. Hazard. Mater*. **2010,** *181*, 666-672.

[3] Liu, J.; Wang, N.; Zhang, H.; Baeyens, J. Adsorption of Congo red dye on $Fe_xCo_{3x}O_4$ nanoparticles. *J. Environ. Manage*. **2019,** *238*, 473-483.

[4] Wu, K.; Pan, X.; Zhang, J.; Zhang, X.; Salah zene, A.; Tian, Y. Biosorption of Congo red from aqueous solutions based on self-immobilized mycelial pellets: kinetics, isotherms, and thermodynamic studies. *ACS Omega*. **2020,** *5*(38), 24601-24612.

[5] Sreeremya, S. Congo red-Review. *Adv. Life Sci*. **2016,** *5*(4), 1123-1126.

[6] Zakaria, M. Z. H.; Baini, R.; Zauzi, N. S. A. Effect of pH, Dosage and concentration on the adsorption of Congo red onto untreated and treated aluminium dross. *Mater. Sci. Eng*. **2017,** *205*, 012026.

[7] Priyadarshini, B.; Patra, T.; Sahoo, T. R. An efficient and comparative adsorption of Congo red and Trypan blue dyes on MgO nanoparticles: Kinetics, thermodynamics and isotherm studies. *J. Magnes. Alloy*. **2021,** *9*(2), 478-488.

[8] Hernández-Zamora, M.; Martínez-Jerónimo, F. Congo red dye diversely affects organisms of different trophic levels: A comparative study with microalgae, cladocerans, and zebrafish embryos. *Environ. Sci. Pollut. Res*. **2019,** *26*(12), 11743-11755.

[9] Nawaz, S.; Siddique, M.; Khan, R.; Riaz, N.; Waheed, U.; Shahzadi, I.; Ali, A. Ultrasound-assisted hydrogen peroxide and iron sulfate mediated Fenton process as an efficient advanced oxidation process for the removal of Congo red dye. *Pol. J. Environ. Stud*. **2022,** *31*(3), 2749-2761.

[10] Saleh, R.; Taufik, A. Degradation of methylene blue and Congo-red dyes using Fenton, photo-Fenton, sono-Fenton,

and sonophoto-Fenton methods in the presence of iron (II, III) oxide/zinc oxide/graphene (Fe_3O_4/ZnO/graphene) composites. *Sep. Purif. Technol*. **2019,** *210*, 563-573.

[11] Gharbani, P.; Tabatabaii, S. M.; Mehrizad, A. Removal of Congo red from textile wastewater by ozonation. *Int. J. Sci. Environ*. 2008, *5*(4), 495-500.

[12] Tapalad, T.; Neramittagapong, A.; Neramittagapong, S.; Boonmee, M. Degradation of Congo red dye by ozonation. *Chiang. Mai. J. Sci*. **2008,** *35*(1), 63-68.

[13] Suhaimi, A.; Mahmoudi, E.; Siow, K. S.; Mohammad, A. W.; MohdRazip Wee, M. F. Nitrogen incorporation by plasma polymerization of heptylamine on PES membrane for removal of anionic dye (Congo red). *Int. J. Sci. Environ*. **2021,** *18*(6), 1443-1452.

[14] Goudjil, S.; Guergazi, S.; Masmoudi, T.; Achour, S. Effect of reactional parameters on the elimination of Congo red by the combination of coagulation-flocculation with aluminium sulfate. *Desalin. Water Treat*. **2021,** *209*, 429-436.

[15] Forgacs, E.; Cserháti, T.; Oros, G. Removal of synthetic dyes from wastewaters: A review. *Environ. Int*. **2004,** *30*(7), 953-971.

[16] Debnath, P.; Mondal, N. K. Effective removal of Congo red dye from aqueous solution using biosynthesized zinc oxide nanoparticles. *Environ. Nanotechnol. Monit. Manag*. **2020,** *14*, 100320.

[17] Namasivayam, C.; Arasi, D. J. S. E. Removal of Congo red from wastewater by adsorption onto waste red mud. *Chemosphere*. **1997,** *34*(2), 401-417.

[18] Stoica-Guzun, A.; Stroescu, M.; Jinga, S. I.; Mihalache, N.; Botez, A.; Matei, C.; Berqer, D.; Damian, C. M.; Ionita, V. Box-Behnken experimental design for chromium (VI) ions removal by bacterial cellulose-magnetite composites. *Int. J. BiolMacromol*. **2016,** *91*, 1062-1072.

[19] Krishnamachari, P.; Hashaikeh, R.; Tiner, M. Modified cellulose morphologies and its composites; SEM and TEM analysis. *Micron*. **2011,** *42*(8), 751-761.

[20] Aljeboree, A. M.; Alshirifi, A. N.; Alkaim A. F. Kinetics and equilibrium study for the adsorption of textile dyes on coconut shell activated carbon. *Arab. J. Chem*. **2017,** *10*(2), 53381-53393.

[21] Sharma, G.; AlGarni, T. S.; Kumar, P. S.; Bhogal, S.; Kumar, A.; Sharma, S.; Naushad, M.; ALOthman, Z. A.; Stadler, F. J. Utilization of Ag_2O-Al_2O_3-ZrO_2 decorated onto rGO as adsorbent for the removal of Congo red from aqueous solution. *Environ. Res*. **2021,** *197*, 111179.

[22] Zhang, F.; Ma, B.; Jiang, X.; Ji, Y. Dual function magnetic hydroxyapatite nano powder for removal of malachite green and Congo red from aqueous solution. *Powder Technol*. **2016,** *302*, 207-214.

[23] Pandey, G.; Singh, S.; Hitkari, G. Synthesis and characterization of polyvinyl pyrrolidone (PVP)-coated Fe_3O_4 nanoparticles by chemical coprecipitation method and removal of Congo red dye by adsorption process. *Int. Nano. Lett*. **2018,** *8*, 111-121.

[24] Roy, T. K.; Mondal, N. K. Potentiality of Eichhornia shoots ash towards removal of Congo red from aqueous solution: isotherms, kinetics, thermodynamics and optimization studies. *Groundw. Sustain. Dev*. **2019,** *9*, 100269.

[25] Zafar, M. N.; Saeed, M.; Nadeem, R.; Sumrra, S. H.; Shafqat, S. S.; Qayyum, M. A. Chemical pretreatments of Trapabispinosa's peel (TBP) biosorbent to enhance adsorption capacity for Pb(II). *Open Chem. J.* **2019,** *17*, 325-336.

[26] Kaya, N. Removal of Congo red and rhodamine B dyes from aqueous solution using unmodified and NH_3/HCl-modified wood charcoal: A kinetic and thermodynamic study. *Fuller. Nanotub. Carbon Nanostr*. **2020,** *29*(3), 183-195.

[27] Yan, Z.; Fu, L.; Yang, H.; Ouyang, J. Amino-functionalized hierarchical porous SiO_2-AlOOH composite nanosheets with enhanced adsorption performance. *J. Hazard. Mater*. **2018,** *344*, 1090-1100.

[28] Weber, T. W.; Chakravorti, R. K. Pore and solid diffusion models for fixed-bed adsorbers. *AIChEJ*. **1974,** *20*, 228-238.

[29] Lin, C.; Qiao, S.; Luo, W.; Liu, Y.; Liu, D.; Li, X.; Liu, M. Thermodynamics, kinetics and regeneration studies for adsorption of Cr (VI) from aqueous solutions using modified cellulose as adsorbent. *Bio Resources*. **2014,** *9*(4), 6998-7017.

[30] Ayawei, N.; Ebelegi, A. N.; Wankasi, D. Modelling and interpretation of adsorption isotherms. *J. Chem*. **2017,** *2017*, 3039817.

[31] Erdogan, F. O. Freundlich, Langmuir, Temkin, D-R and Harkins-Jura isotherm studies on the adsorption of CO_2 on various porous adsorbents. *Int. J. Chem. React. Eng*. **2018,** *17*(5), 134.

[32] Dubinin, M. The potential theory of adsorption of gases and vapors for adsorbents with energetically nonuniform surfaces. *Chem. Rev*. **1960,** *60*(2), 235-241.

[33] Sips, R. Combined form of Langmuir and Freundlich equations. *J. Chem. Phys*. **1948,** *16*, 490-495.

[34] Ho, Y. S.; McKay, G. Pseudo-second-order model for sorption processes. *Process Biochem*. **1999,** *34*(5), 451-465.

[35] Kajjumba, G. W.; Emik, S.; Öngen, A.; Özcan, H. K.; Aydın, S. Modelling of adsorption kinetic processes-errors, theory and application. In *Advanced Sorption Process Applications*; Edebali S., Ed.; IntechOpen, 2018, pp 187-206.

[36] Arrhenius, S. On the influence of carbonic acid in the air upon the temperature of the ground. *Lond. Edinb. Dubl. Phil. Mag.* **1896,** *41*(251), 237-276.

[37] Toumi, I.; Djelad, H.; Chouli, F.; Benyoucef, A. Synthesis of PANI@ ZnO hybrid material and evaluations in adsorption of Congo red and methylene blue dyes: structural characterization and adsorption performance. *J. Inorg. Organomet. Polym. Mater*. **2022,** *32*(1), 112-121.

[38] Fegade, U.; Kolate, S.; Dhake, R.; Inamuddin, I.; Altalhi, T.; Kanchi, S. Adsorption of Congo Red on Pb doped Fe_xO_y: experimental study and theoretical modeling via double-layer statistical physics models. *Water Sci. Technol*. **2021,** *83*(7), 1714-1727.

[39] Khalaf, I. H.; Al-Sudani, F. T.; AbdulRazak, A. A.; Aldahri, T.; Rohani, S. Optimization of Congo red dye adsorption from wastewater by a modified commercial zeolite catalyst using response surface modeling approach. *Water Sci. Technol*. **2021,** *83*(6), 1369-1383.

[40] Jabar, J. M.; Odusote, Y. A.; Alabi, K. A.; Ahmed, I. B. Kinetics and mechanisms of Congo red dye removal from aqueous solution using activated Moringa oleifera seed coat as adsorbent. *Appl. Water Sci.* **2020,** *10*, 136.

[41] Malik, A.; Khan, A. A.; Anwar, N.; Naeem, M. A. Comparative study of the adsorption of Congo red dye on rice husk, rice husk char and chemically modified rice husk char from aqueous media. *BCSE*. **2020,** *34*(1), 41-54.

[42] Inkoua, S.; Maloko, H. L.; Koko, M. M.; Yan, L. Facile solvothermal synthesis of Fe_3O_4/magnetic grapefruit peel for adsorptive removal of Congo red, humic acid and phosphate from aqueous solutions. *Material Express*. **2020,** *10*(1), 37-44.

[43] Obaid, R. M.; Hassan, S. A. Removal of Congo red and bromophenol red dyes from aqueous solutions by adsorption onto a low-cost adsorbent: Pomegranate seeds wastes. *AIP Conference Proceedings*. **2020,** *2290*(1), 030016.